

Air Force Institute of Technology

AFIT Scholar

Faculty Publications

11-2018

Evaluation of Eu:LiCAF for Neutron Detection Utilizing SiPMs and Portable Electronics

Michael A. Ford

Buckley E. O'Day III

John W. McClory

Air Force Institute of Technology

Manish K. Sharma

Areg Danagoulian

Follow this and additional works at: <https://scholar.afit.edu/facpub>



Part of the [Electrical and Electronics Commons](#), and the [Nuclear Engineering Commons](#)

Recommended Citation

Ford, Michael A., et al. "Evaluation of Eu:LiCAF for Neutron Detection Utilizing SiPMs and Portable Electronics." *Nuclear Instruments and Methods in Physics Research Section A: Accelerators, Spectrometers, Detectors and Associated Equipment*, vol. 908, Nov. 2018, pp. 110–16, <https://doi.org/10.1016/j.nima.2018.08.016>

This Article is brought to you for free and open access by AFIT Scholar. It has been accepted for inclusion in Faculty Publications by an authorized administrator of AFIT Scholar. For more information, please contact richard.mansfield@afit.edu.

Evaluation of Eu:LiCAF for neutron detection utilizing SiPMs and portable electronics

Michael A. Ford^a, Buckley E. O'Day^a, John W. McClory^a, Manish K. Sharma^c, Areg Danagoulian^b

^a*Air Force Institute of Technology, Department of Engineering Physics, 2950 Hobson Way, Wright-Patterson AFB, OH 45433*

^b*Massachusetts Institute of Technology, Department of Nuclear Science and Engineering, 77 Massachusetts Ave, Cambridge, MA 02139*

^c*University of Michigan, Department of Nuclear Engineering and Radiological Sciences, 2355 Bonisteel Boulevard, Ann Arbor, MI 48109*

Abstract

With the increasing cost and decreasing availability of ^3He , there have been many efforts to find alternative neutron detection materials. Lithium calcium aluminum fluoride (LiCAF) enriched to 95% ^6Li doped with europium was evaluated here as a replacement material for ^3He . Wafers 0.5 cm thick, consisting of LiCAF crystals in a rubberized matrix, were embedded with wavelength shifting fibers (WSF) and mated to silicon photo-multipliers (SiPMs) to measure the photon response in a flux of neutrons from a DD neutron generator. Excellent discrimination was realized between neutrons and gammas, and both pulse-height discrimination and pulse-shape analysis were explored. A Figure of Merit (FoM) of 1.03 was achieved. By applying pulse-shape analysis, a simple neutron count output was generated by utilizing a low-pass filter to suppress fast pulses from the SiPM output and subsequently applying a threshold to the remaining signal. Custom electronics were built to bias the SiPMs, then amplify, filter, discriminate, and digitize the LiCAF/WSF scintillation photons, resulting in a digital pulse that can easily be counted with any microcontroller or field programmable gate array. A significant advantage of LiCAF is that it can be fabricated into any shape/size (when embedded in a rubberized matrix),

Preprint submitted to NIM-A

July 15, 2018

and the light output and transparency is sufficient to allow for thicker scintillators which enable detection of both thermal and epithermal neutrons. This work demonstrated that Eu:LiCAF is capable of discriminating gammas from neutrons and is a potential replacement material for ^3He , especially for nuclear security applications and neutron spectroscopy.

Keywords: Neutron Detection, LiCAF, Pulse Shape Analysis

1. Introduction

Neutron detection has been investigated for decades, and it has been an enduring goal of the nuclear community to develop accurate and inexpensive neutron detection and spectroscopy techniques. The goal of this work was to focus on a detection medium that can effectively replace ^3He based neutron detectors, while also possessing properties that allow it to perform well as a neutron counter in a layered neutron spectrometer setup. ^3He has long been the material of choice for detecting neutrons, but high cost and limited supplies have created the impetus to find a replacement material. LiCAF (lithium calcium aluminum fluoride) is the material of choice for this work because of its desirable properties: non-hygroscopic, low γ sensitivity, available in larger sizes, transparent and high light yield [1, 2]. $\text{ZnS}:\text{}^6\text{LiF}$ and $\text{ZnS}:\text{}^{10}\text{B}_2\text{O}_3$ are other alternatives that have been recently studied, and while ZnS has many desirable properties as a scintillator, there are also significant disadvantages including a long afterglow time (upwards of $100\ \mu\text{s}$) and opacity to its own light [3]. ^{10}B based neutron detectors have the advantage of a larger neutron interaction cross section, however, the reaction products are lower energy than ^6Li and include gammas [4].

LiCAF has been previously evaluated by Viererbl et al. and separately by the Pacific Northwest National Laboratory (PNNL) [1, 2]. Viererbl et al. focused on the ability to discriminate signals from neutron and gamma radiation

22 and PNNL evaluated LiCAF for application in a portal monitoring system. Us-
23 ing only pulse-height analysis, Viererbl et al. found that gamma radiation with
24 energies above 1400 keV started to interfere with the neutron peak from a 0.5 cm
25 thick wafer of Eu:LiCAF [2]. The discrimination capability, however, is highly
26 dependent on the size and density of small grains (scintillator crystals) in the
27 rubber, and also the geometry of the detector. PNNL found that the LiCAF
28 neutron detector's sensitivity for a bare and moderated ^{252}Cf source is 1.01
29 ± 0.09 and 1.54 ± 0.23 cps/ng respectively with large rubberized Eu:LiCAF
30 detectors measuring 100 cm long, 26 cm wide and 3 cm thick [1]. This is ap-
31 proximately 40-60% of the value suggested as a requirement for portal monitors
32 [5].

33 Wafers of rubberized Eu:LiCAF were obtained from Tokuyama Corpora-
34 tion, Japan. First, the wafers were evaluated for their neutron response and
35 the ability to discriminate neutrons from gammas. Wavelength shifting fibers
36 (WSF) from Kuraray (B-3) were embedded in the wafers to convert the scintil-
37 lation photons to a frequency that is optimized for SensL C-Series blue-sensitive
38 silicon photo-multipliers (SiPMs). SiPMs have been used for many years in ap-
39 plications ranging from medical imaging, 3D ranging and sensing, biophotonics,
40 high energy physics, and now for threat identification [6–9]. The scintillation
41 light of particle detectors has historically been collected with traditional photo-
42 multiplier tubes. However, recent advances have significantly reduced the dark
43 noise of SiPMs. Coupling the low dark noise with the greater transparency
44 and relatively high light output of LiCAF creates ideal conditions to introduce
45 SiPMs to inelastic neutron scattering detectors [10].

46 Previous work with LiCAF indicates that it has the ability to perform well
47 as a neutron detector. The scintillation properties of LiCAF make it desirable
48 for use with silicon photo-multipliers because of its high light output, excellent

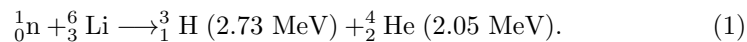
49 transparency, and ability to discriminate neutrons from gammas. Custom elec-
50 tronics were developed as part of this work to readout, amplify, filter, and count
51 the neutron pulses created in LiCAF by a neutron flux. The methodology and
52 results are discussed herein.

53 **2. LiCAF Scintillator**

54 Two compositions of LiCAF are available from the Tokuyama Corporation.
55 It is available doped with europium or cerium, has an effective Z of 15 and
56 density of 2.99 g/cm³ [11]. There are a few primary differences between the
57 dopants that led to Eu:LiCAF being chosen for this work. The light yield of
58 Eu:LiCAF is approximately eight times that of Ce:LiCAF. The decay constant
59 of Ce:LiCAF is 40 ns, while it is >1 μ s for Eu:LiCAF. This is a disadvantage
60 of Eu:LiCAF, as the shorter decay constant is desirable, however, since the
61 material was tested in environments with a relatively low neutron flux, the
62 longer decay constant was not a significant issue. The luminescent wavelength
63 of the Eu:LiCAF is 360-390 nm as compared to the Ce:LiCAF at 280-320 nm.
64 The optimal wavelength for the Sensl-C series silicon photo-multiplier is the
65 peak sensitivity region (approximately 425 nm) where the photon detection
66 efficiency (PDE) is at 42% with an overvoltage of 5.0 V [12]. The photon
67 detection efficiency is highly dependent on the overvoltage of the SiPMs. Finally,
68 europium has a much larger neutron absorption cross section than cesium does,
69 especially near the thermal energy region [13]. This is a disadvantage of the
70 europium atoms, but it is not a serious issue because of the trace amounts of
71 atoms that are present only in the Eu:LiCAF fibers embedded in the rubberized
72 wafer; the primary interaction with the europium is (n, γ) and the gammas will
73 not significantly interact with the low-Z material.

74 Eu:LiCAF/rubber (2×10^{21} ⁶Li/cm³) was used throughout this work. The

75 neutron absorption percentage of the rubber-matrix LiCAF is approximately
 76 5% higher than ^3He at 10 atm for 25 meV neutrons [11]. While the neutron
 77 absorption percentage is much larger for the pure LiCAF crystal, since it is
 78 largely dependent on the number of ^6Li atoms, the cost of the material is an
 79 order-of-magnitude higher. The neutron absorption percentage of pure cerium
 80 or europium doped LiCAF crystal is $\sim 60\%$ for a 1 mm thick sample (thermal
 81 neutrons), whereas it is only $\sim 17\%$ for the Eu:LiCAF/rubber used for this work.
 82 Thermal neutrons have a high cross section for absorption in ^6Li resulting in
 83 the following reaction:



84 Both the tritium and the alpha particles interact in the LiCAF crystal scintilla-
 85 tor, emitting photons that are transported via the WSFs to the SiPMs, where
 86 a current is created. The current is then amplified and converted to a voltage
 87 signal, then filtered and converted to a digital signal using a comparator. The
 88 digital signals can then be counted/recorded using a field-programmable gate
 89 array (FPGA) or microcontroller.

90 A disadvantage of Eu:LiCAF is the relatively low α/β ratio. The difference
 91 between the ratio of absorbed energy and the light yield for the gamma radia-
 92 tion and heavy charged particles (HCP) is caused by the quenching dependence
 93 on the linear energy transfer (LET). The ratio for Eu:LiCAF is 0.2 [14]. This
 94 presents an issue for bulk Eu:LiCAF crystals, as the scintillation light from the
 95 high-energy HCPs is approximately equivalent to a 1 MeV gamma. The discrim-
 96 ination problem can be mitigated by controlling the geometry of the crystals
 97 since the range of the fast electrons induced by gamma rays is significantly
 98 longer than the HCP range. In the case of the rubberized LiCAF, controlling
 99 the size of the small LiCAF grains embedded in the rubber matrix is essential,

100 and also the number and spacing of the small grains to optimize discrimination
101 capability while not significantly sacrificing neutron detection efficiency. Using
102 a smaller grain size of LiCAF in the rubber matrix is advantageous for discrim-
103 ination purposes as it allows the fast electrons induced by gamma rays to easily
104 escape the scintillator grain before depositing their full energy [15]. Another
105 method of controlling the sensitivity to gammas is by reducing the overall Li-
106 CAF in the wafers (reducing the number of small grains). A drawback to the
107 lower density of LiCAF is the reduced neutron detection efficiency.

108 Each wafer of rubberized Eu:LiCAF scintillator used throughout this work
109 is $10 \times 10 \text{ cm} \times 0.5 \text{ cm}$ thick. There are also 30 WSF fibers embedded in both
110 the X and Y axes through the wafer. The WSFs are desirable for signal readout
111 because of the flexibility of the rubberized LiCAF and the custom geometries,
112 which makes using traditional PMTs difficult to implement. However, the gam-
113 mas and neutrons tend to interact with the WSFs (as they are very similar
114 to plastic scintillation fibers) [15]. [15] found that the spectrum obtained from
115 the WSFs without the Eu:LiCAF scintillator is almost the same as the one ob-
116 tained with the Eu:LiCAF scintillator and the WSFs when using a ^{60}Co gamma
117 source. The gamma/WSF signals are an undesirable side-effect of utilizing the
118 wavelength-shifting fibers, however the scintillation pulses of the WSFs are on
119 the order of nanoseconds, and an active low-pass filter will be utilized through-
120 out this work to discriminate the gamma/WSF signals from the neutron pulses
121 ($\sim 1 \mu\text{s}$).

122 **3. Electronics**

123 Maintaining the portability of the detectors was a primary consideration in
124 designing the electronics for the pulse counting and discrimination. Traditional
125 PMTs were not used because of their size and power requirements; SiPMs of-

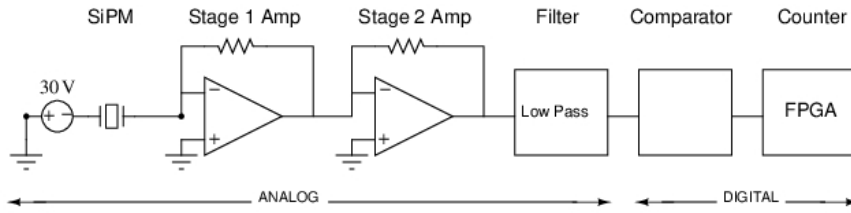


Figure 1: Schematic showing the signal flow through the LiCAF pulse counter circuit.

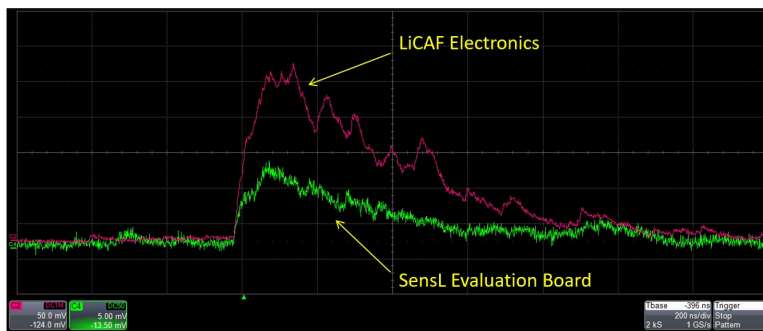


Figure 2: Comparison of the output signals from BGO scintillator using the SensL evaluation board and the portable electronic readout employing the Analog Devices AD8007.

126 fer similar specifications as PMTs without many of the disadvantages [6–9].
 127 The advantage of using SiPMs is that they are extremely small, are insensi-
 128 tive to magnetic fields, operate ideally with relatively low voltage (30 V), and
 129 the output signal can be easily amplified and filtered with basic electronics.
 130 A disadvantage of SiPMs is that their detection efficiency and gain are highly
 131 dependent on temperature.

132 A schematic of the pulse counter circuit is shown in Fig. 1. The timing
 133 and gain of each component was carefully chosen to ensure that proper pulse-
 134 shape filtering and amplification can be achieved. The first essential component
 135 is the Sensl C-Series SiPM, which has a microcell size of $35 \mu m$ and a peak
 136 sensitivity of 425 nm. The stage 1 is a simple npn transistor used to buffer
 137 the current (unity gain) from the SiPMs and the stage 2 amplifier is an Analog

138 Devices AD8007 (ultralow distortion high-speed amplifier, 650 MHz, 1000 V/ μ s
139 slew rate) with a gain of +2. Initial testing was conducted with the SensL
140 evaluation board (MicroFC-SMA-300xx-35u) to ensure that the light emitted
141 from the LiCAF would result in a sufficiently high signal-to-noise ratio (SNR)
142 after the inefficiencies from both the WSFs and the photon detection efficiency
143 of the SiPMs (maximum of 42%). Fig. 2 shows the results from comparing the
144 SensL evaluation board to the custom circuit using a BGO crystal and ^{68}Ge
145 gamma source. A BGO scintillator was used for the early electronic testing
146 because it has a well documented light output from the 511 keV annihilation
147 gammas that could be used for comparison in simulations. The original signal
148 from the evaluation board (green trace, 5 mV/div) had a peak amplitude of
149 about 10 mV, whereas the custom circuit using the AD8007 amplifier (red trace,
150 50 mV/div) had a peak amplitude of approximately 250 mV and a faster slew
151 rate with the same BGO crystal.

152 The signal shown in Fig. 2 is collected at the output of the stage 2 amplifier;
153 it then must go through a filter, comparator, and finally a counter. The purpose
154 of the filter after the amplifiers was to suppress the faster pulses in the rubberized
155 Eu:LiCAF wafer and WSFs. The gamma/WSF pulses have a higher frequency
156 than the neutrons, thus filtering the faster pulses, in conjunction with pulse-
157 height discrimination, allowed most of the gamma/WSF pulses to be rejected.
158 An active low-pass filter was developed using the Analog Devices ADA4857-
159 1 Operational Amplifier. This amplifier was chosen because of its desirable
160 properties: ultralow distortion, low power, low noise, and high speed. The
161 next step after the filter was to perform pulse-height discrimination. This was
162 done with the Maxim Integrated MAX995, high speed, low voltage comparator.
163 The comparator outputs a digital pulse anytime the user-defined threshold was
164 exceeded. Using a micro-controller or field programmable gate array, the rising

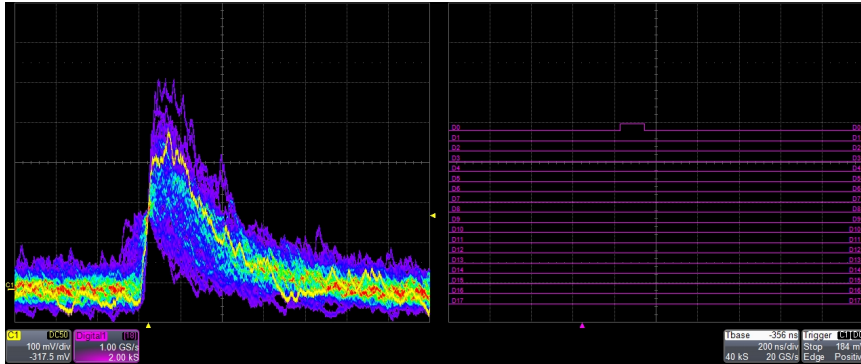


Figure 3: Persistent oscilloscope traces of the electronic circuit mated to a $4\text{mm} \times 4\text{mm}$ BGO crystal with a ^{68}Ge gamma source (left), and the output digital pulse from the MAX995 comparator (right). The digital output (right) is not in persistence mode and shows a digital pulse whenever the threshold voltage is exceeded.

165 edges of the comparator output can be counted to determine the number of
 166 neutrons that interacted with the LiCAF. The comparator was setup in burst
 167 guard mode, which limits pulse pile-up. Counts were only recorded when the
 168 pulse signal amplitude exceeded the user-defined threshold.

169 Modeling of the circuit was performed using LTSpice, and the circuit was
 170 validated using a BGO crystal with a ^{68}Ge source. BGO has a lower light out-
 171 put and slower decay time than other available crystals (such as LYSO), which
 172 would more accurately reflect the properties of LiCAF. While LiCAF does emit
 173 approximately 40,000 photons per neutron [16], many of the photons are not
 174 collected in the fibers, or are lost in the transmission process. Fig. 3 shows the
 175 persistent oscilloscope traces of the output of the stage 2 amplifier (left column
 176 of scope image), and the right column of the scope image shows the comparator
 177 output due to the gamma interaction in the BGO. The digital output of Fig. 3
 178 (right) is not in persistence mode and only shows a pulse each time the compar-
 179 ator threshold voltage is exceeded. The LTSpice simulation of the circuit
 180 matched in amplitude, pulse shape, and rise time with the experimental results.

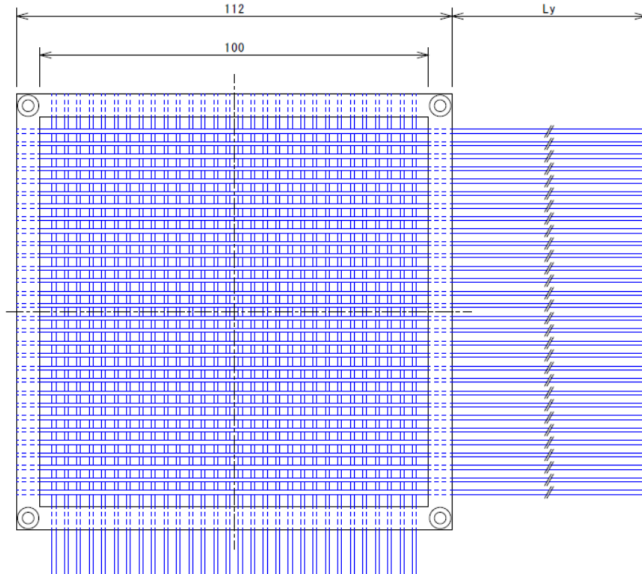


Figure 4: CAD drawing of the LiCAF wafer from Tokuyama.

181 4. Experiment

182 A sample 10×10 cm wafer of rubberized Eu:LiCAF was evaluated. The
 183 wafer was 0.5 cm thick and had WSF (polystyrene matrix and organic phosphor)
 184 embedded along both the X and Y-axes. There were 30 one mm diameter fibers
 185 embedded on each axis (Fig. 4) to allow for position-dependent readout, and
 186 to provide a sufficient number of photons reaching the SiPMs. It is generally
 187 accepted that only about 1% of the wavelength shifted photons will reach the
 188 SiPMs after accounting for the collection efficiency and re-emission of photons
 189 along the axial direction of the fibers [10]. A light-tight box was placed around
 190 the entire wafer/electronics assembly to minimize the number of ambient pho-
 191 tons interacting with the SiPMs, which served to keep the signal-to-noise ratio
 192 as large as possible. To further reduce the number of ambient photons that have
 193 the potential to decrease the SNR, caps were 3-D printed out of a black nylon
 194 (PA 11) to fit tightly over the SiPM, while only having one extrusion at the top

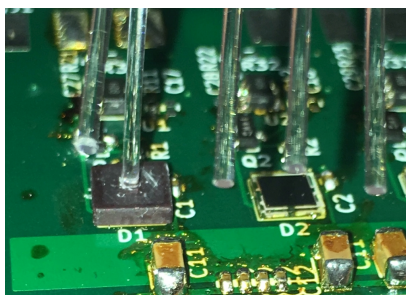


Figure 5: Mating of the fibers to the SiPMs using 3-D printed caps and optical glue.

195 to allow the fiber to fit tightly (Fig. 5). The 3-D cap was also used as a way to
196 mount and hold the fiber in place while the optical glue dried (Loctite 349). The
197 electronics used to amplify the SiPM signal required +/-5 V, ground, negative
198 high voltage (approximately 30 V [12]), and a variable reference voltage for the
199 comparator. The output of the electronics was either an SMA cable or a single
200 wire for the digital pulse, depending on the analysis being performed. The SMA
201 cable allowed output of the waveforms for post-processing, or the digital pulses
202 can be used if neutron counts are the only interest.

203 Although the rubberized Eu:LiCAF has very low sensitivity to gammas,
204 gamma interactions do occur. Because of the fast-signal suppression of the
205 WSF scintillation events, the relatively small LiCAF grain size and density, and
206 the fact that the neutrons deposit more energy in the scintillator (from the high
207 energy and low range of the alpha particle and triton), the two sources can be
208 very effectively distinguished using the combination of filtering and pulse-height
209 discrimination.

210 Data was taken through two experiments: one at the Air Force Institute
211 of Technology using an Adelphi Technology DD108 Neutron Generator. The
212 DD108 produces ~ 2.45 MeV neutrons at a continuous emission rate of 1×10^9
213 n/s with 100 kV accelerating voltage, an operating beam current of 3 mA and

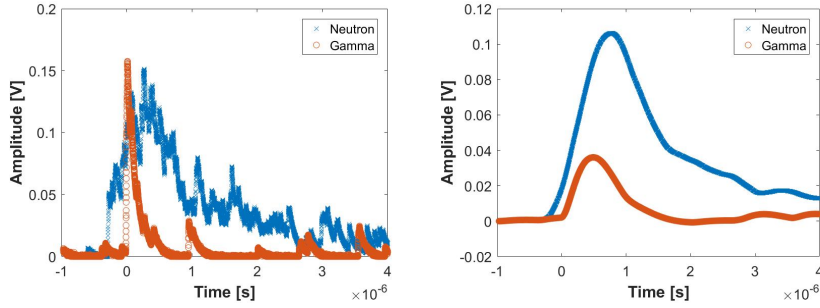


Figure 6: Digitization of the gamma/WSF and neutron pulse before being filtered (left) and after a low-pass filter (right). In this case, the pre-filter pulse amplitude of the neutron is less than the pre-filter amplitude of the gamma/WSF. After filtering, pulse-height discrimination can be used to eliminate the gamma/WSF because of the fast-pulse suppression.

214 deuterium flow rate of 8.0 SCCM [17]. The second set of tests were conducted
 215 at the University of Michigan using a Thermo Scientific MP320 DD neutron
 216 generator with an emission rate of 1×10^6 n/s, and also a ^{252}Cf source with
 217 a calculated activity of 2.77×10^6 Bq [18]. For the neutron generators, a single
 218 LiCAF wafer was placed perpendicular to the isotropic flow of neutrons from
 219 the core of the generator at a distance of 20 cm. Testing with the ^{252}Cf source
 220 was conducted with the source 25 cm from the front face of the LiCAF wafer.

221 4.1. Pulse Height Discrimination

222 Initial testing with the rubberized Eu:LiCAF wafer concentrated on using
 223 pulse-height discrimination, in conjunction with pulse-shape filtering, to allow
 224 a simple neutron count output. Three sets of data were taken with a single
 225 WSF in the center of a LiCAF wafer. Background neutron counts were negli-
 226 gible. The first test collected 3000 digitized traces using a ^{137}Cs source placed
 227 directly adjacent to the wafer. Data was taken with an SMA cable output ter-
 228 minating into a Teledyne WaveRunner 620Zi oscilloscope. MATLAB was used
 229 for post-processing and the area under each of the pulses was integrated (inte-
 230 grated energy) and plotted. Integrated energy was used as a metric since the

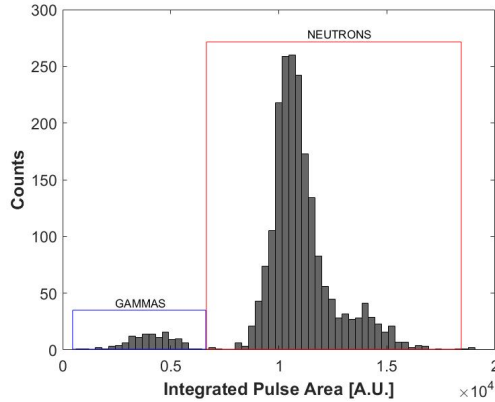


Figure 7: The LiCAF detector is able to discriminate neutrons from gammas and WSF scintillation events using pulse-shape analysis followed by pulse-height discrimination. This is the result of capturing waveforms for a 5 minute test run with both ^{137}Cs and the DD Generator.

231 current generated by the SiPM is proportional to the number of photons col-
 232 lected; integrating the area of the pulse gives a linear correlation to the energy
 233 deposited in the scintillator. The next test recorded 3000 traces again, this time
 234 using only the DD generator. Fig 6 shows that the area of the neutron pulses is
 235 significantly larger than the area of the gamma/WSF pulses. From Fig. 6 (left),
 236 the original amplitude of the two pulses from the gamma/WSFs and neutrons
 237 are approximately the same amplitude (so close that pulse-height discrimina-
 238 tion is impractical). However, after filtering the two pulses (an active low-pass
 239 filter with $f_c = 360$ kHz was used), the amplitude of the higher frequency
 240 gamma/WSF pulse is reduced to less than half the amplitude of the neutron
 241 pulse as shown in Fig. 6 (right). Pulse-height discrimination can now be applied
 242 and the gamma/WSF count rejected. The threshold value was experimentally
 243 adjusted with the LiCAF until the gamma/WSF counts were minimized with-
 244 out significantly affecting the number of neutron counts. For simplicity, the
 245 threshold value was decreased until the gamma/WSF counts were less than the
 246 square root of the neutron counts.

247 A final data set was collected for 5 minutes with both the ^{137}Cs and the
 248 DD generator, generating the results shown in Fig. 7. Because of the differ-
 249 ences in timing properties of the gamma/WSFs and neutrons in the wafers, the
 250 high-energy reaction products of the neutron interaction with ^6Li , and the low
 251 LiCAF density in the rubberized matrix, good discrimination can be accom-
 252 plished. The lower energy counts (left peak of Fig. 7) are the faster pulses
 253 from the gammas/WSFs and the peak on the right is the result of the larger,
 254 slower neutron pulses. The peak on the right side of Fig. 7 has a total of
 255 3204 counts, whereas the peak on the left has 63. The total counts for both
 256 gamma/WSFs and neutrons is 3267, and this is the value that would be used
 257 for “neutron counts” in a spectroscopy application. When setting a pulse-height
 258 threshold, it is not practical to raise the threshold so high as to eliminate all
 259 of the gamma/WSF counts, instead, the goal is to raise it high enough as to
 260 keep the gamma/WSF counts at or below the square root of the total counts
 261 (below counting statistics). For this test, the reported counts is 3267 ± 58 neu-
 262 trons, which is approximately consistent with the number of hits in the right
 263 peak of Fig. 7. A 70 mV threshold value was set to maintain the gamma/WSF
 264 counts below the error of the neutron counts for the collection time and activity
 265 of sources used. An overview of the testing results is shown in Table 1. The
 266 results show that there is negligible addition to the neutron counts with the
 267 addition of the ^{137}Cs source.

Table 1: Neutron/gamma discrimination performance using comparator threshold of 70 mV.

Test	cps
Background	<0.01
^{137}Cs	0.103
DD Generator	10.7
DD Generator + ^{137}Cs	10.7

268 The comparator’s threshold voltage was set with an HP 3245A precision
269 voltage supply. The electronics have the ability to output the pulse waveform
270 via an SMA cable, however, once the threshold value is determined it is no longer
271 necessary to use the waveform output. The comparator will output a CMOS
272 pulse anytime the threshold voltage is exceeded. For use in spectroscopy, only
273 the digital output would be necessary and any pulse counter could be employed
274 to tally the number of neutrons captured in the LiCAF.

275 4.2. Pulse-Shape Analysis

276 The focus of testing at the University of Michigan was to determine the rub-
277 berized Eu:LiCAF wafer’s ability to discriminate neutrons from gammas and
278 WSF scintillation events using only pulse-shape analysis. Pulse-shape analysis
279 was applied to separate gammas and WSF scintillation events from neutron
280 waveforms based on the traditional charge integration method. The peak of
281 each waveform was found, and an integration window on each side of the peak
282 was selected to find the area of the peak down to a user-specified threshold
283 level. A Figure of Merit (FoM) was utilized to evaluate the ability of the rub-
284 berized Eu:LiCAF wafer to discriminate the neutrons from the gammas and
285 WSF scintillation events. The FoM was defined as:

$$\text{FoM} = \frac{d}{FWHM_n + FWHM_\gamma} \quad (2)$$

286 where d is the distance between the centroids ($\mu_n - \mu_\gamma$) of the gamma and neutron
287 peaks when the integrated energy of the waveforms are plotted on the same
288 axis via a histogram, and the $FWHM_n$ and $FWHM_\gamma$ are the full width half-
289 maximum (2.35σ) of the neutron and gamma peaks of the histogram, determined
290 by approximating each peak with a Gaussian fit.

291 A one-hour DD neutron generator run was first conducted to evaluate the

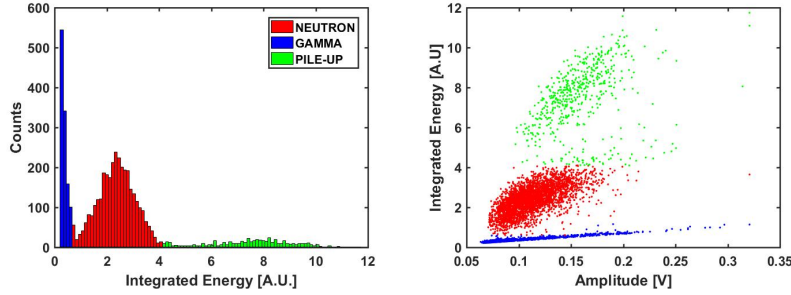


Figure 8: Histogram showing the integrated energy of each waveform from a one-hour DD neutron generator run at the University of Michigan (left). Scatter plot showing integrated area versus pulse-height of each waveform from the one-hour DD neutron generator run (right). Regardless of the gamma/WSF pulse-height, the faster rising edge and lower integrated area of the gamma/WSF event allows the neutrons to be easily discriminated from the gammas.

292 effectiveness of pulse-shape analysis with the rubberized Eu:LiCAF. A LiCAF
 293 wafer was placed adjacent to the target plane of the generator with 2.5 cm of
 294 HDPE placed between the LiCAF wafer and the generator tube. The waveforms
 295 were digitized with a Hantek 6074BE PC oscilloscope and post-processing was
 296 accomplished using MATLAB. The resulting histogram is shown in Fig. 8 (left).
 297 There are three visible peaks in the histogram. The leftmost peak (blue) is a
 298 result of the gammas striking the LiCAF crystal or WSFs and causing scintil-
 299 lation photons to be emitted, or fast-electron interactions in the WSFs. The
 300 central peak (red) is a result of neutron (and a few gamma) interactions in the
 301 LiCAF. The tail of the neutron pulses is, on average, much longer than the
 302 tail of the gamma/WSFs resulting in a larger area. Finally, the rightmost peak
 303 (green) is a result of pulse pile-up in the LiCAF and is indicative of downtime in
 304 the electronics. To compute the FoM, the peaks were separated into respective
 305 histograms for neutrons and gammas (Fig. 9 shows the neutron histogram).
 306 After fitting the histograms with Gaussian curves, the FoM can be calculated.
 307 An overview of the fitting parameters is shown in Table 1.

308 The gamma histogram is partially skewed at lower energies. This is a result

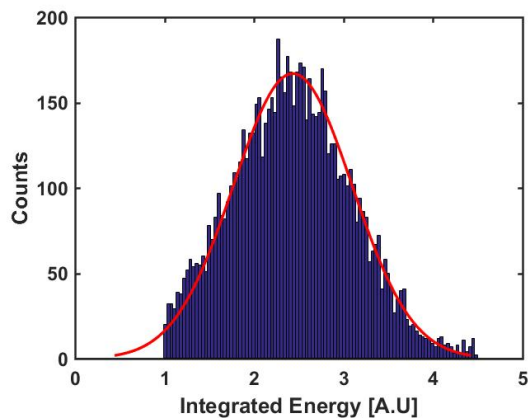


Figure 9: When the neutron pulses are separated from the gamma/WSF pulses in Fig. 8 (left), the histogram can be fitted to a Gaussian curve allowing extraction of μ_n and σ_n to determine the FoM.

Table 2: Specifications of discrimination and Gaussian fit parameters.

Property	DD	^{252}Cf
Baseline Discrimination Level	10 mV	10 mV
μ_n	2.433	2.678
μ_γ	0.410	0.507
σ_n	0.664	0.610
σ_γ	0.169	0.182
FoM	1.033	1.167

309 of the discrimination method that was used to calculate the integrated energy.
310 With a low-level discrimination, there is a minimum area that will be represented
311 and this feature is evident in the histogram. Using the parameters from the
312 Gaussian fits, the FoM of the discrimination was calculated to be 1.03 for the
313 DD generator. Plotting the integrated energy versus the pulse-height represents
314 the capability of pulse-shape analysis using rubberized Eu:LiCAF. Fig. 8 (right)
315 shows a clear distinction between the gamma/WSF waveforms (bottom), the
316 neutron waveforms (middle) and the pile-up waveforms (top). Table 1 also
317 shows data from the ^{252}Cf source. The FoM of the ^{252}Cf is better than the

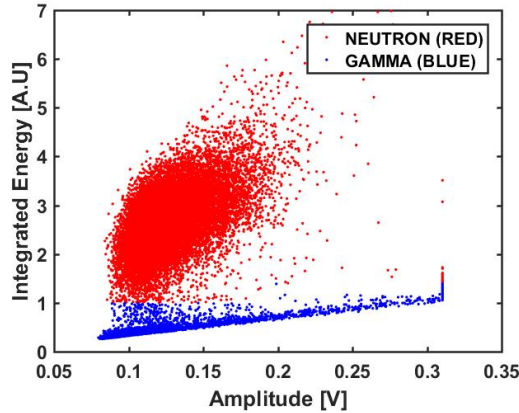


Figure 10: Scatter plot showing integrated area versus pulse-height of each waveform from a 15 hour data collection period with a ^{252}Cf source.

318 DD generator because of the lower average energy neutrons and longer data
 319 collection time. It is also worthy to note that the scatter plot for the ^{252}Cf (Fig.
 320 10) does not have the “pile up” region that is evident in Fig. 8 (right) from the
 321 DD generator.

322 For neutron spectroscopy applications, this analysis shows that pulse-shape
 323 analysis is possible, however, a disadvantage of using the analysis is that it
 324 requires digitization and/or integration of each waveform to determine if the
 325 pulse was a result of a neutron or gamma/WSF interaction. Because each layer
 326 of rubberized Eu:LiCAF has 60 optical fibers for signal read-out, the amount
 327 of instrumentation required to analyze each waveform and perform live pulse-
 328 shape analysis is difficult in practice, hence pulse-height discrimination may be
 329 the preferred method in a layered spectrometer system.

330 5. Conclusions

331 LiCAF shows potential to replace ^3He in many neutron detection applica-
 332 tions. While a pure LiCAF crystal was not evaluated here, the scintillation pho-

333 tons are easily detectable in the rubberized form with commercial off-the-shelf
334 (COTS) SiPMs. In addition, discrimination between neutrons and gammas can
335 be performed using simple and compact electronics which would enable highly
336 mobile applications. LiCAF shows promise using both pulse-height discrimina-
337 tion and pulse-shape analysis. Pulse-height discrimination allowed for a simple
338 neutron-count output where the gamma counts were below the neutron count-
339 ing statistics, and a FoM of 1.03 was demonstrated using pulse-shape analysis
340 with the DD neutron generator. The FoM with a ^{252}Cf source was calculated
341 to be 1.17.

342 One of the key considerations with using SiPMs is the SNR. Often times,
343 the small signal of SiPMs can get lost in high noise environments, whether from
344 photon noise from improper shielding of the SiPMs or electronic noise induced
345 in the circuit. Care must be taken to properly amplify the current pulse of the
346 SiPM (done herein with a transimpedance amplifier), then filter the resulting
347 voltage signal. A threshold applied to the pulse height then allows for pulse-
348 height discrimination, and digital pulses can then be counted, and recorded
349 as neutron “hits”. The flexible shape of rubberized LiCAF and the use of
350 compact SiPMs instead of traditional, bulkier PMTs allows for the creation
351 of custom, palm-sized neutron spectrometers requiring no more than a single
352 battery to power. Future testing with LiCAF will include assembly of a ten-layer
353 spectrometer utilizing pulse-height discrimination to count neutrons and the
354 incident neutron energy will be determined via spectrum unfolding. Additional
355 testing will be done with only the polystyrene matrix and organic phosphor
356 WSFs to evaluate how they react as stand-alone scintillation detectors.

357 6. Acknowledgments

358 This work was supported at the Air Force Institute of Technology by the
359 Defense Threat Reduction Agency (HDTRA17-245-26). Views expressed in this
360 paper are those of the authors and do not necessarily reflect the official policy
361 or position of the Air Force, the Department of Defense, or the United States
362 Government.

363 [1] M. Woodring, R. Kouzes, M. Demboski, R. Cameron, J. Magana, Charac-
364 terization of the Tokuyama Corporation LiCAF Neutron Detector, Tech.
365 rep., Pacific Northwest National Laboratory (2015). doi:PNNL-ACT-10032.

366 [2] L. Viererbl, V. Klupák, M. Vinš, M. Kolečka, J. Šoltés, A. Yoshikawa,
367 M. Nikl, LiCaAlF₆ scintillators in neutron and gamma radiation fields,
368 International Journal of Modern Physics: Conference Series 44 (2016)
369 1660234. doi:10.1142/S2010194516602349.

370 URL [http://www.worldscientific.com/doi/abs/10.1142/
371 S2010194516602349](http://www.worldscientific.com/doi/abs/10.1142/S2010194516602349)

372 [3] T. Nakamura, M. Katagiri, N. Tsutsui, K. Toh, N. J. Rhodes, E. M. Schoon-
373 eveld, H. Ooguri, Y. Noguchi, K. Sakasai, K. Soyama, Development of a
374 ZnS/10B₂O₃ scintillator with low-afterglow phosphor, Journal of Physics:
375 Conference Series 528 (1). doi:10.1088/1742-6596/528/1/012043.

376 [4] F. D. Amaro, C. M. B. Monteiro, J. M. F. dos Santos, A. An-
377 tognini, Novel concept for neutron detection: proportional counter filled
378 with 10B nanoparticle aerosol, Scientific Reports 7 (1) (2017) 41699.
379 doi:10.1038/srep41699.

380 URL <http://www.nature.com/articles/srep41699>

381 [5] R. T. Kouzes, J. H. Ely, A. T. Lintereur, E. K. MacE, D. L. Stephens,
382 M. L. Woodring, Neutron detection gamma ray sensitivity criteria, Nuclear

- 383 Instruments and Methods in Physics Research, Section A: Accelerators,
384 Spectrometers, Detectors and Associated Equipment 654 (1) (2011) 412–
385 416. doi:10.1016/j.nima.2011.07.030.
386 URL <http://dx.doi.org/10.1016/j.nima.2011.07.030>
- 387 [6] M. Foster, D. Ramsden, A compact neutron detector based on the use of
388 a SiPM detector, IEEE Nuclear Science Symposium Conference Record
389 (2008) 1882–1886doi:10.1109/NSSMIC.2008.4774758.
- 390 [7] J. B. Mosset, A. Stoykov, U. Greuter, M. Hildebrandt, N. Schlumpf, H. Van
391 Swygenhoven, Evaluation of two thermal neutron detection units consisting
392 of ZnS/ ^6LiF scintillating layers with embedded WLS fibers read out with
393 a SiPM, Nuclear Instruments and Methods in Physics Research, Section
394 A: Accelerators, Spectrometers, Detectors and Associated Equipment 764.
395 doi:10.1016/j.nima.2014.07.060.
- 396 [8] A. Stoykov, J. B. Mosset, U. Greuter, M. Hildebrandt, N. Schlumpf,
397 A SiPM-based ZnS: ^6LiF scintillation neutron detectorarXiv:1408.6119,
398 doi:10.1016/j.nima.2015.01.076.
399 URL <http://arxiv.org/abs/1408.6119>[http://dx.doi.org/10.1016/](http://dx.doi.org/10.1016/j.nima.2015.01.076)
400 [j.nima.2015.01.076](http://dx.doi.org/10.1016/j.nima.2015.01.076)
- 401 [9] S. Gnechchi, C. Jackson, A 1 16 SiPM Array for Automotive 3D Imaging
402 LiDAR Systems, International Image Sensor Society (2017) 133–136.
- 403 [10] N. Rhodes, Scintillation Detectors, Neutron News (23) (2012) 26.
- 404 [11] K. Fukuda, Scintillators Developed by Tokuyama for Neutron Detection
405 Functional Fluoride Group, Tech. rep., Tokuyama Corporation (2014).
- 406 [12] SensL, C-Series Low Noise , Fast , Blue-Sensitive Silicon Photomultipliers,
407 Tech. rep., SensL Corporation (2014).

- 408 [13] IAEA, ENDF - Europium Neutron Total Cross Section.
409 URL <https://www-nds.iaea.org/exfor/servlet/E4sSearch2>
- 410 [14] D. Sugimoto, K. Watanabe, K. Hirota, A. Yamazaki, A. Uritani,
411 T. Iguchi, K. Fukuda, S. Ishidu, N. Kawaguchi, T. Yanagida, Y. Fuji-
412 moto, A. Yoshikawa, H. Hasemi, K. Kino, Y. Kiyonagi, Neutron TOF
413 Experiments Using Transparent Rubber Sheet Type Neutron Detector
414 with Dispersed Small Pieces of LiCaAlF₆ Scintillator, Physics Procedia 60
415 (2014) 349–355. doi:10.1016/J.PHPRO.2014.11.047.
416 URL [https://www.sciencedirect.com/science/article/pii/
417 S187538921400594X](https://www.sciencedirect.com/science/article/pii/S187538921400594X)
- 418 [15] K. Watanabe, T. Yamazaki, D. Sugimoto, A. Yamazaki, A. Uri-
419 tani, T. Iguchi, K. Fukuda, S. Ishidu, T. Yanagida, Y. Fujimoto,
420 Wavelength-shifting fiber signal readout from Transparent RUBber
421 SheeT (TRUST) type LiCaAlF₆ neutron scintillator, Nuclear Instru-
422 ments and Methods in Physics Research Section A: Accelerators,
423 Spectrometers, Detectors and Associated Equipment 784 (2015) 260–263.
424 doi:10.1016/J.NIMA.2014.11.109.
425 URL [https://www.sciencedirect.com/science/article/pii/
426 S0168900214014235](https://www.sciencedirect.com/science/article/pii/S0168900214014235)
- 427 [16] T. Yanagida, A. Yamaji, N. Kawaguchi, Y. Fujimoto, K. Fukuda, S. Kuro-
428 sawa, A. Yamazaki, K. Watanabe, Y. Futami, Y. Yokota, A. Uritani,
429 T. Iguchi, A. Yoshikawa, M. Nikl, Europium and Sodium Codoped Li-
430 CaAlF₆ Scintillator for Neutron Detection, Applied Physics Express
431 4 (10) (2011) 106401. doi:10.1143/APEX.4.106401.
432 URL <http://stacks.iop.org/1882-0786/4/106401>

- 433 [17] Adelphi, DD108 Neutron Generator Adelphi Technology.
434 URL <http://www.adelphitech.com/products/dd108.html>
- 435 [18] Thermo Scientific, Thermo Scientific MP 320 Lightweight, Portable
436 Neutron Generator Thermo Scientific MP 320 Neutron Generator.
437 URL <https://assets.thermofisher.com/TFS-Assets/CAD/Specification-Sheets/D10497{~}.pdf>
438